American Mineralogist, Volume 85, pages 89–102, 2000

An investigation of matrix effects in the analysis of fluorine in humite-group minerals by EMPA, SIMS, and SREF

LUISA OTTOLINI,[1,*] FERNANDO CÁMARA,[1,†] AND SIMONA BIGI[2]

[1]CNR-CENTRO DI STUDIO PER LA CRISTALLOCHIMICA E LA CRISTALLOGRAFIA, VIA FERRATA 1, I-27100 PAVIA, ITALY
[2]DIPARTIMENTO DI SCIENZE DELLA TERRA, UNIVERSITÀ DEGLI STUDI DI MODENA, LARGO S. EUFEMIA 19, I-41100 MODENA, ITALY

ABSTRACT

Accurate determination of F in minerals is a difficult task even when high F concentrations are present. Fluorine usually is determined by means of electron micro-probe analysis (EMPA) standardized on non-silicate-matrix compounds (e.g., fluorite), and some previous work has revealed the difficulties in determining F at high concentrations such as found in the humite-group minerals. Moreover, when both single-crystal structure refinement (SREF) and EMPA are available for the same crystal, the two estimates do not always agree. On the other hand, the secondary ion mass spectrometry (SIMS) technique is not easily applied at high F concentrations due to the existence of matrix effects related to the chemical composition and structure of the sample as well as to the concentration of the element itself. We tested the agreement among these analytical techniques in the estimation of high F contents and propose an analytical procedure for the analysis of fluorine. Our results indicate that careful selection of working conditions for EMPA of F together with appropriate correction, can yield accurate fluorine concentrations in minerals. Fluorine data extracted from refined site occupancies are systematically overestimated. New accurate working curves have been worked out for SIMS analysis of F taking Si and Mg, in turn, as the reference element for the matrix. Humite-group minerals show SIMS matrix effects on the order of ~10%. In analyzing fluoborite in the most unfavorable cases, the difference in Ion Yield (F/Mg) between "disoriented" humite-group minerals and "oriented" fluoborite samples can reach ~27%. Finally, a lower than expected IY(F/Si) from the F/Si working curve (made with humite minerals) is shown by topaz, which can be ascribed to chemical matrix effects, as well as to the covalent-type bonding between F and the major element in the matrix (Al).

INTRODUCTION

Precise and accurate determination of F in minerals is far from being completely and routinely achieved. Usually F in minerals, glasses, and other geological materials is determined by means of EMPA. This technique, however, is limited by several factors such as: low count-rates using large single-crystal reflectors (e.g., TAP) in wavelength-dispersive spectrometry, and interferences from the higher-order lines of heavier elements (Raudsepp 1995); the presence of "matrix effects" related to high X-ray absorption in the specimen; the lack of suitable standards; peak shifts and changes in peak shape between chemically and structurally dissimilar specimens (Solberg 1982).

A considerable improvement in terms of count rate has recently been achieved by means of the new LSM reflectors, i.e., layered synthetic microstructures (Potts and Tindle 1989). They give better peak-to-background ratios [an improvement of 14 times for the F$K\alpha$ with a W/Si ($2d$ = 60 Å) microstructure], but they possess lower resolving power than TAP (Fialin et al. 1993). With these new reflectors, multiple-order interferences greater than the second-order are absent (e.g., the third-order P$K\alpha$ peak in apatite). Nevertheless, interferences due to second-order peaks from Mg and Al and first-order L-lines from Fe still survive and constitute a limitation in the determination of fluorine in minerals rich in Mg, Al, and transition elements (Raudsepp 1995).

Matrix effects on light elements have been accounted for with the development of $\phi(\rho z)$ programs (Bastin and Heijligers 1991; Goldstein et al. 1992; Reed 1996). Accurate analysis of elements such O, N, C, and B have been reviewed in some papers and monographs by Bastin and Heijligers (1986a, 1986b, 1986c, 1986d, 1988, 1989, 1991). However, very little information has been published on the problems concerning the analysis of the heaviest of the light elements, i.e., F. Moreover, the accuracy of mass-absorption coefficients could be a source of error in the correction of intensity data.

The valence electrons of light elements affect K emission (Fialin et al. 1993; Raudsepp 1995), which produces dramatic changes in peak shape and peak shifts. Those changes have been reported for B$K\alpha$ (Bastin and Heijligers 1991). Additionally, the peak position can depend strongly on the crystallographic orientation of a particular sample. Anyway, all those effects are less

* E-mail: ottolini@crystal.unipv.it
† Present address: Laboratoire Structure & Proprietes Etat Solide, Université Sciences & Technologies de Lille, Bat C6, 59655 Villeneuve d'Ascq-Cedex, France.

severe for elements with higher atomic number. To overcome this analytical problem, it would be necessary to integrate the peak area, which is very time-consuming. One alternative method is to use area peak factors (APFs) (Bastin and Heijligers 1986a, 1986b, 1986c, 1986d). The APF is calculated starting from one standard and one unknown sample (S and U, respectively) where APF = $(I^{I}_{U} I^{P}_{S})/(I^{P}_{U} I^{I}_{S})$. I^{I}_{U} is the integrated intensity of the unknown; I^{P}_{S} is the peak-intensity of the standard; I^{P}_{U} is the peak-intensity of the unknown; and I^{I}_{S} is the integrated intensity of the standard.

The effects of crystallographic orientation on F*K*α X-ray intensity in apatite have been reported by Stormer et al. (1993) under beam conditions routinely used for EMPA (15 kV, 15 nA). On the (001) section of apatite, the F*K*α intensity increases by a factor of two during the first 60–120 seconds, followed by a decrease over the next 360 seconds toward a constant value; on (100) sections, the F*K*α intensity increases by ~20% over the same period. A different behavior was shown by topaz, analyzed in both orientations, i.e., (001) and (100), and fluorite in unknown orientation. Reducing the beam current reduces the variation in intensity, but also decreases the overall intensity and thus analytical precision.

Fluorine can also be analyzed using positive or negative secondary ions by means of SIMS. Not much data have been available until now. One of the first attempts to analyze F^+ secondary ions at low emission-energies in humite-group minerals (clinohumite, norbergite, chondrodite) and amphiboles was the study of Hinthorne and Andersen (1975). The working curve F(Si), where Si represents the matrix reference element, was relatively straightforward for the silicate standards (with F contents determined by EMPA).

In spite of the relatively high ionization potential, i.e., 17.42 eV, F^+ ions are surprisingly intense at low secondary-ion energies, probably due to the high efficiency with which secondary electrons can desorb F ions from the sample (Williams 1992). When high-energy ions are studied, the sensitivity for F decreases and its ion yield relative to Si—IY(F/Si), (IY = relative ion intensity to relative atomic concentration ratio)—also decreases (Ottolini et al. 1994); the IY(F/Si) is two orders of magnitude lower than that of other light elements such as, for instance, Li which has a IY(Li/Si) ~1.5 (Ottolini et al. 1993). The primary control of relative sensitivity in SIMS is a steep exponential function of ionization potential and not mass of a particular element as in X-ray emission techniques such as EMPA.

The presence of matrix effects and the lack of well-characterized standards have hampered F quantification. Matrix effects in SIMS are a complex function of the chemical composition, crystal structure, and/or orientation of the matrix. They depend on the concentration of the element itself and that of the major elements in the matrix. Due to the complexity of the sputtering/ionization process, matrix effects cannot be predicted for a given mineral chemistry and they generally change with changing matrix composition. As for structural and orientation matrix effects, no systematic F investigation has been carried out by SIMS until now, so that a mention of matrix effects typically refers to chemical matrix effects.

Examples of SIMS matrix effects in F-bearing crystals and glasses are known (Hervig unpublished data; Kovalenko et al. 1988). The lack of linearity between ion intensity and EMPA concentrations has been observed in the analysis of F in topaz (Hervig et al. 1987). In other cases, two non-linear relations between atomic F/(F + OH) from the bulk-chemical analysis and the ratio F/(F + H) from secondary ion intensities were obtained from muscovite and phlogopite-biotite (Jones and Smith 1984).

Using high-energy positive secondary ions reduces the influence of non-linear effects on the ionization of light elements such as Li, Be, and B (Ottolini et al. 1993). Under the same instrumental conditions, a working curve for F in silicates (kornerupine, phlogopite, and amphibole) ranging from 0.1 to 2.9 wt%, plus one topaz with 20.3 wt% F, was also obtained by Ottolini et al. (1994). The measured points fall along a line with a ±20% deviation from F concentrations measured by EMPA. Therefore preliminary results showed matrix effects in these samples on the order of about ±20% rel. (including analytical errors from EMPA), which were mainly ascribed to the chemical composition in the absence of a controlled sample orientation.

Another example of a calibration curve for F^+ in rhyolite glasses was reported by Ihinger et al. (1994) using secondary ions with 75 ± 20 eV kinetic energy normalized to the $^{30}Si^+$ count rate. Negative secondary ions of F are much more intense than positive ones: 1 count/second F^- for less than 1 ppm of F using a 1 nA O^- primary beam and secondary ions with energies of 50 ± 20 eV. The calibration curve, constructed with the same rhyolite samples (Ihinger et al. 1994), plus one F-rich amphibole and three different apatites, shows a slope greater by a factor of 1.3 than that for the rhyolite glasses only. The authors' conclusion was that the extent of matrix effects for this element remains to be investigated.

With the aim of gaining an insight into the matrix effects affecting the microanalysis of F, we selected humite-group minerals [$n Mg_2SiO_4 \cdot Mg(F,OH)_2$, Penfield and Howe 1894, where $n = 1$ stands for norbergite, $n = 2$ for chondrodite, $n = 3$ for humite, and $n = 4$ for clinohumite], and analyzed them by EMPA, SREF, and SIMS. These minerals can be used to investigate matrix effects on the F (and H) ionization. Providing no other substitutions are present, the humites represent a magnesium-silicate matrix with an approximately constant Si/Mg ratio and a variable quantity of OH or F. However, with these compositions it is not possible to isolate the interrelationship between Si and Mg; therefore a fluoborite [$Mg_3(OH,F)_3(BO_3)$] sample was selected. Fluoborite presents a very simple composition in which MgO (wt%) and Mg (at) are similar to that in humite-group minerals. The studied sample is F-enriched, which allows matrix effects to be evaluated. The previously used topaz (Ottolini et al. 1994) has been added to this set of samples to compare the fluorine ion yield between Mg- and Al-basis matrices, and to derive information about F sputtering/ionization mechanisms in different F-rich matrices.

The results of the present work have allowed us to evaluate the influence of chemical composition, crystal structure, and crystal orientation on F measurement. On this basis, an analytical protocol for the measurement of high F levels in humite-group minerals by means of microanalytical techniques is proposed below.

Experimental procedures

Sample description

We studied a series of samples with similar chemical composition but increasing F content. The samples come from metamor-

phosed and metasomatized marbles from Huerta del Vinagre, a small scheelite deposit cropping out in the Guadaiza Unit of the Upper Alpujarride series, in the Betic Cordillera. They are (in order of increasing F content): clinohumite, chondrodite, and norbergite (in the following cited as Chum HV-41 n.2, Chum HV-41 n.3, Chond HV-43 n.3, Chond HV-43 n.4, and Norb HV-47 n.7, respectively). Two more norbergite crystals (cited as Norb HV-43 n.4 and Norb HV-47 n.1), previously studied by Cámara (1997), were added to the set. We also checked two partially OH– substituted fluoborite crystals (cited as Fbor HV-43 n.2 and n.3; Cámara and Ottolini 2000) and two topaz crystals from Topaz Mountain, Utah (kindly provided by R. Hervig and already investigated by Ottolini et al. 1994). All of these samples should provide a variety of chemical compositions, including major elements other than Mg as B, Si, and Al.

Humite-group minerals are orthosilicates, which can be summarized (Gibbs and Ribbe 1969; Jones et al. 1969; Gibbs et al. 1970) as a slightly distorted hexagonal close-packed (HCP) anion array containing zigzag edge-sharing octahedral chains scrolling parallel to the *c* axis and cross linked by isolated SiO_4 tetrahedra. The ratio between tetrahedral and octahedral voids in HCP is 2/1 (half of the tetrahedra point up, the rest point down). In all humite-group minerals half of octahedral voids are occupied by M^{2+} cations; the tetrahedral voids are variably occupied in each different mineral. Their structures were first determined by Taylor and West (1928, 1929) who found them to be monoclinic (chondrodite and clinohumite) and orthorhombic (norbergite and humite) with the space groups $P2_1/b$ and *Pbnm*. The non-standard cell orientation is taken in reference to the olivine cell.

Fluoborite is classified as the simplest borate consisting of homopolyhedral clusters of triangular coordination BO_3 polyhedra. It belongs to the 3 Å wallpaper structure group of Moore and Araki (1974), and consists of pairs of edge-sharing infinite octahedral chains, forming ribbons along [001] cross-linked by BO_3 triangles.

Topaz is an orthosilicate consisting of isolated SiO_4 tetrahedra linked with pairs of edge-sharing octahedra. It represents a low-silicon silicate in which the dominant element is Al. Usually it occurs in nature as the F-type end-member. However, the fully hydrated end-member, known as "topaz-OH," has been synthesized experimentally (Wunder et al. 1993).

X-ray analysis, data collection, and structure refinement

The crystals for SREF were handpicked from crushed pieces of rock on the basis of their optical behavior. The data collection was carried out with an automated 4-circle Philips PW1100 diffractometer, using graphite-monochromatized Mo$K\alpha$ radiation. Standard working conditions were 60 kV and 25 mA. Unit-cell dimensions were calculated from least-squares refinement of the position of 60 rows of reflections in the range $-35 < \theta < 35°$. Values for the clinohumite and chondrodite crystals studied are reported in Table 1. The profiles were integrated following the method of Lehmann and Larsen (1974), modified by Blessing et al. (1974). Data were corrected for Lorentz polarization and absorption following North et al. (1968) and the equivalent reflections were averaged and reduced to structure factors. Merging *R*-factors are presented in Table 1.

Only unit-cell parameters were determined on the topaz crystals because they were already embedded in epoxy. A position-sensitive diffractometer (Nonius FAST system) equipped with a Mo rotating anode generator was used to determine unit-cell dimensions. The standard cell-refinement routines included in the software provided with the diffractometer were used (MADNES, Messerschmidt and Pflugrath 1987). Weighted full-matrix, least-squares refinements were carried out using a modified version of ORFLS (Busing et al. 1962) for all crystals but Norb HV-47 n.1 and Norb HV-43 n.3, which were refined by Cámara (1997) using SHELXL-93 (Sheldrick 1993). Scattering factors were taken from *International Tables for Crystallography* (Wilson 1992): in particular, neutral vs. ionized scattering-factors were used for O site (Ungaretti et al. 1983); F^- vs. O^- for the O5 site; vacancy vs. H in the H site; and Mg^{2+} vs. Fe^{2+} in M1, M2, and M3 octahedral sites. We refined neutral vs. ionized scattering factors in sites with only one chemical species, following Hawthorne et al. (1995). A difference-Fourier map showed some residual maxima. The most important residuals were identified as the bonding electrons between the Si-O and the B-O bonds.

Atomic coordinates, equivalent isotropic atomic displacement parameters (adp), and refined site scattering are reported in Table 2; selected interatomic distances in Table 3; observed and calculated structure factors in Table 4; and anisotropic components of the adp in Table 5[1].

TABLE 1. Selected crystal and refinement data

	Chond HV-43 n.3	Chond HV-43 n.4	Chum HV-41 n.2	Chum HV-41 n.3
mineral	chondrodite	chondrodite	clinohumite	clinohumite
code	fwf	gaq	fhb	gap
a (Å)	4.7230(9)	4.7226(9)	4.7405(12)	4.7396(12)
b (Å)	10.2584(28)	10.2564(28)	10.2377(39)	10.2328(39)
c (Å)	7.8504(33)	7.8490(33)	13.6496(4)	13.6439(4)
α (°)	109.076(24)	109.076(24)	100.843(27)	100.843(27)
V (Å^3)	359.47	359.47	650.61	650.61
Z	2	2	2	2
R_{sym}	1.7	1.5	1.3	1.9
no. ref. par.*	88	88	143	143
2θ range (°)	2-70	2-60	2-70	2-60
R_w	2.21(1642)	2.49(1092)	1.88(2624)	2.65(1889)
GoF	0.984	1.237	0.997	0.994
$R_{3\sigma}$	1.39(1550)	1.78(1043)	1.41(2411)	1.80(1760)

Note: Code = symbolic address in the CSCC database; R_{sym} = merging agreement factor; R_w = weighted refinement agreement factor; GoF = Goodness of Fit.
* Number of refined parameters.

Electron microprobe analyses

The crystals were mounted in epoxy resin, polished, and carbon-coated. They were analyzed for cations (Si, Mg, Fe, Mn, Ti, Ca, Al, Cr), and F and Cl with an ARL-SEMQ Electron Microprobe at Dipartimento di Scienze della Terra, University of Modena. The following mineral standards were used for calibration: clinopyroxene KHl (Si, Ca,); spessartite (Mn, Al); ilmenite (Ti, Fe); Spring Water olivine (Mg); Canada blue sodalite (C1);

[1]For a copy of Tables 4 and 5, Document item AM-00-030, contact the Business Office of the Mineralogical Society of America (see inside front cover of recent issue) for price information. Deposit items may also be available on the American Mineralogist web site at http://www.minsocam.org.

TABLE 2. Atomic fractional coordinates, equivalent isotropic atomic displacement parameters (Å^2), and refined site scattering (epfu)

atom	s.s.*	x/a		y/b		z/c		B_{eq}
				Chum HV-41 n.2				
O1,1	8.00	0.73294	(14)	0.06451	(7)	0.38811	(5)	0.41
O1,2	8.00	0.27787	(15)	0.41947	(6)	0.38776	(5)	0.40
O1,3	8.00	0.22308	(15)	0.11240	(7)	0.29312	(5)	0.43
O1,4	8.00	0.22238	(15)	0.15881	(7)	0.48636	(5)	0.43
O2,1	8.00	0.23624	(14)	0.32276	(7)	0.16287	(5)	0.40
O2,2	8.00	0.77897	(15)	0.96885	(6)	0.16257	(5)	0.44
O2,3	8.00	0.72430	(15)	0.27994	(7)	0.26273	(5)	0.45
O2,4	8.00	0.72808	(15)	0.22680	(7)	0.07021	(5)	0.45
O5	8.57	0.26152	(15)	0.04630	(6)	0.05566	(5)	0.68
Si1	14.00	0.07329	(5)	0.06623	(2)	0.38930	(2)	0.31
Si2	14.00	0.07641	(5)	0.17670	(2)	0.83511	(2)	0.31
M1,A	12.28	0.5		0		0.5		0.46
M1,B	12.29	0.49743	(7)	0.94627	(3)	0.27421	(2)	0.48
M2,5	12.23	0.00928	(7)	0.14038	(3)	0.17026	(2)	0.49
M2,6	12.28	0.50876	(7)	0.25023	(3)	0.38825	(2)	0.45
M3	12.40	0.49277	(7)	0.87792	(3)	0.04299	(2)	0.52
H	0.35	0.067	(17)	–0.021	(8)	0.013	(6)	4.51
				Chum HV-41 n.3				
O1,1	8.00	0.73319	(18)	0.06451	(8)	0.38810	(6)	0.38
O1,2	8.00	0.27818	(18)	0.41946	(8)	0.38781	(6)	0.42
O1,3	8.00	0.22349	(18)	0.11244	(8)	0.29321	(6)	0.43
O1,4	8.00	0.22232	(18)	0.15885	(8)	0.48631	(6)	0.44
O2,1	8.00	0.23585	(18)	0.32291	(8)	0.16289	(6)	0.40
O2,2	8.00	0.77862	(18)	0.96886	(8)	0.16249	(6)	0.43
O2,3	8.00	0.72435	(18)	0.27998	(8)	0.26271	(6)	0.42
O2,4	8.00	0.72776	(18)	0.22658	(8)	0.07007	(6)	0.45
O5	8.59	0.26193	(18)	0.04644	(8)	0.05568	(6)	0.67
Si1	14.00	0.07341	(7)	0.06624	(3)	0.38934	(2)	0.32
Si2	14.00	0.07655	(7)	0.17672	(3)	0.83514	(2)	0.31
M1,A	12.35	0.5		0		0.5		0.51
M1,B	12.30	0.49760	(8)	0.94628	(4)	0.27423	(3)	0.50
M2,5	12.22	0.00935	(9)	0.14043	(4)	0.17024	(3)	0.50
M2,6	12.35	0.50894	(9)	0.25023	(4)	0.38823	(3)	0.49
M3	12.41	0.49291	(9)	0.87778	(4)	0.04305	(3)	0.52
H	0.32	0.084	(18)	0.001	(10)	0.021	(7)	4.35
				Chond HV-43 n.3				
O1	8.00	0.77761	(13)	0.00156	(6)	0.29407	(8)	0.46
O2	8.00	0.72731	(12)	0.24074	(6)	0.12567	(8)	0.42
O3	8.00	0.22439	(12)	0.16824	(6)	0.52798	(8)	0.41
O4	8.00	0.26401	(12)	0.85487	(6)	0.29478	(8)	0.39
O5	8.79	0.26227	(12)	0.05742	(5)	0.10053	(7)	0.68
Si	14.00	0.07656	(5)	0.14403	(2)	0.70374	(3)	0.35
M1	12.79	0.5		0		0.5		0.52
M2	12.39	0.00943	(6)	0.17358	(3)	0.30654	(4)	0.49
M3	12.38	0.49214	(6)	0.88645	(3)	0.07927	(4)	0.49
H	0.38	0.143	(11)	0.024	(6)	0.021	(8)	3.79
				Chond HV-43 n.4				
O1	8.00	0.77749	(19)	0.00158	(9)	0.29381	(12)	0.48
O2	8.00	0.72730	(19)	0.24078	(9)	0.12569	(12)	0.45
O3	8.00	0.22456	(19)	0.16834	(9)	0.52795	(12)	0.45
O4	8.00	0.26413	(19)	0.85492	(9)	0.29496	(12)	0.42
O5	8.76	0.26252	(19)	0.05756	(9)	0.10064	(11)	0.73
Si	14.00	0.07642	(7)	0.14413	(3)	0.70375	(5)	0.37
M1	12.61	0.5		0		0.5		0.51
M2	12.32	0.00936	(9)	0.17352	(4)	0.30652	(6)	0.50
M3	12.31	0.49218	(9)	0.88645	(4)	0.07939	(6)	0.50
H	0.27	0.100	(13)	0.016	(7)	0.023	(9)	0.41

* s.s. = site scattering in electrons.

chromite (Cr); fluorite (F). Analytical results are included in Tables 6a, 6b, and 7.

Orientation of crystals

To investigate the possible role of crystal orientation on F$K\alpha$ X-ray emission and fluorine ionization, we determined the different crystal orientations with a diffractometer before embedding the grains in epoxy. For such a task we used a position sensitive detector (PSD) Nonius FAST system at CNR-CSCC (Pavia). Up to 250 reflections were collected in two Phi rotations separated by 90° and the unit cell was determined and refined. We used the "ORIENT" level of MADNES (Messerschmidt and Pflugrath 1987) to get the crystals in the required orientation. Afterward, the crystals were mounted in this orientation.

In humite-group minerals, fluorine is concentrated in bands perpendicular to *b* axis; therefore, the angle between the inci-

TABLE 3. Selected interatomic distance (Å) and geometrical parameters

	Chum HV-41 n.2	Chum HV-41 n.3		Chond HV-43 n.3	Chond HV-43 n.4
<Si1-O>	1.636	1.635	<Si-O>	1.632	1.632
Vol (Å^3)	2.212	2.208	Vol (Å^3)	2.196	2.197
TQE*	1.011	1.011	TQE	1.010	1.010
TAV	49.31	49.19	TAV	44.71	45.24
<Si2-O>	1.635	1.635	<M1-O>	2.106	2.106
Vol (Å^3)	2.208	2.209	Vol (Å^3)	11.968	11.965
TQE	1.0102	1.0102	OQE	1.027	1.027
TAV	45.66	45.30	OAV	98.77	98.18
<M1,A-O>	2.096	2.096	<M2-O>	2.117	2.116
Vol	11.809	11.86	Vol	12.256	12.244
OQE	1.026	1.026	OQE	1.022	1.022
OAV	93.63	93.85	OAV	74.86	74.83
<M1,B-O>	2.102	2.1009	<M3-O>	2.081	2.080
Vol (Å^3)	11.892	11.874	Vol (Å^3)	11.72	11.711
OQE	1.0275	1.0274	OQE	1.018	1.018
OAV	98.46	98.41	OAV	58.32	58.18
<M2,5-O>	2.118	2.118	H-H	1.443	1.030
Vol (Å^3)	12.284	12.284	O5-H	0.825	0.9835
OQE	1.0217	1.0218			
OAV	73.15	73.15			
<M2,6-O>	2.130	2.128			
Vol (Å^3)	12.403	12.382			
OQE	1.0266	1.0266			
OAV	91.14	91.33			
<M3-O>	2.084	2.082			
Vol (Å^3)	11.762	11.735			
OQE	1.0184	1.0182			
OAV	60.56	60.26			
H-H	0.8796	0.9723			
O5-H	1.2318	1.0363			

Notes: σ (standard deviation) on distance <0.001 Å; TAV = tetrahedral angle variance; TQE = tetrahedral quadratic elongation; OAV = octahedral angle variance; OQE = octahedral quadratic elongation.
* Following Robinson et al. (1971).

TABLE 6a. Fluorine EMPA data on the studied crystals at 7 keV with and without APF correction (APFs included in table)

			no APF		with APF		
mineral		crystal orient.	F wt%	2σ%	F wt%	2σ%	APF
Chum	HV-41 n.2	general	2.82	17.0	3.15	17.0	1.12
	HV-41 n.3	pall. to b axis	3.06	4.6	3.45	4.6	1.13
Chond	HV-43 n.3	general	6.03	4.4	6.27	4.4	1.04
	HV-43 n.4	pall. to b axis	6.75	6.5	7.53	5.8	1.13
Norb	HV-47 n.7	general	12.27	3.8	13.42	3.8	1.10
	HV-43 n.4	pall. to b axis	13.87	4.6	15.17	4.7	1.12
	HV-47 n.1	pall. to b axis	13.70	3.7	15.48	3.8	1.14
Topaz	T1	pall. to b axis	16.29	4.1	20.89	4.1	1.50
	T2	pall. to c axis	15.01	3.0	19.53	3.0	1.53
Fbor	HV-43 n.3	perp. to c axis	21.05	2.8	22.19	2.8	1.06

TABLE 6b. Fluorine EMPA data on the studied crystals at 15 keV with and without APF correction (APFs included in table)

			no APF		with APF		
mineral		crystal orient.	F wt%	2σ%	F wt%	2σ%	APF
Chum	HV-41 n.2	general	3.28	8.0	3.92	7.8	1.19
	HV-41 n.3	pall. to b axis	2.88	15.6	3.19	15.4	1.10
Chond	HV-43 n.3	general	5.97	7.1	6.98	7.1	1.16
	HV-43 n.4	pall. to b axis	6.00	3.5	7.00	3.5	1.16
Norb	HV-47 n.7	general	13.40	6.7	14.32	6.6	1.08
	HV-43 n.4	pall. to b axis	12.71	4.5	14.46	4.4	1.16
	HV-47 n.1	pall. to b axis	12.97	6.2	14.74	6.2	1.08
Topaz	T1	pall. to b axis	16.56	4.3	23.01	4.1	1.50
	T2	pall. to c axis	15.95	2.2	22.56	2.2	1.53
Fbor	HV-43 n.3	perp. to c axis	22.26	3.2	23.30	3.3	1.06
	HV-43 n.2	pall. to c axis	20.31	5.5	22.38	5.5	1.13

dent electron beam and those planes was calculated for each crystal. Crystals Norb HV-43 n.4, Norb HV-47 n.1 (Cámara 1997), Chum HV-41 n.3, and Chond HV-43 n.4 were embedded with *b* axis parallel to the incident electron beam, whereas Chum HV-41 n.2 and Chond HV-43 n.3 were embedded in a general position with none of their cell-axes parallel to the incident electron beam. Norb HV-47 n.7 was mounted with its *a* axis at 35° to the electron beam, Fbor HV-43 n.3 and Fbor HV-43 n.2, with their *c* axis perpendicular and parallel to the incident electron beam, respectively. The two topaz crystals (T1: $a = 4.661$ Å, $b = 8.835$ Å, and $c = 8.402$ Å; T2: $a = 4.654$ Å, $b = 8.811$ Å, and $c = 8.408$ Å) had the following orientation: T1, *b* axis sub-parallel to the incident electron beam (13.45°); T2, *c* axis sub-parallel to the incident electron beam (6.7°). For T1 the planes with maximum density of fluorine atoms are nearly parallel to the analysis surface. For T2 those planes are nearly parallel to the incident electron beam (thus perpendicular to the analysis surface). A scheme of the relationship between crystal structure, ion, and electron beam is shown in Figure 1.

Ion microprobe analyses

SIMS investigations were carried out using a Cameca IMS 4f ion microprobe, installed at CNR-CSCC, Pavia. The samples were gold coated (~300 Å thickness) before analysis. In commercial instruments, such as ours, the primary ion beam hits the sample obliquely at an incidence angle of 60°, i.e., the optical axis of the primary column makes an angle of 30° to the normal of the sample (Cameca Manual, "Cameca ion microprobe IMS3f–Physical Principles").

The experimental procedure involved a $^{16}O^-$ primary ion beam with 2 nA current intensity and a ~ 5 μm beam diameter. ^{19}F, ^{24}Mg, and ^{30}Si isotopes were monitored as secondary positive ions with medium-high emission kinetic energies (in the range ~75–125 eV), according to the method of Ottolini et al. (1993) developed for light-element analysis. Secondary ions were selected by offsetting the sample accelerating voltage by –100 V while keeping constant the settings of the electrostatic analyzer (ESA) voltages and the width and position of the energy slit (±25 eV). In its conventional configuration, energy filtering (CEF) allows the elimination of molecular ions due to their different energy distribution with respect to monatomic ions in the medium- to high-energy region of mass spectrum. The CEF technique is not effective for the suppression of multiply charged ions and hydrides. To keep the moisture in the samples as low as possible, they were stored for several days under rotary-pump vacuum before analysis. Nevertheless, "energy-filtered" F^+ secondary ions were checked at a mass resolution of ~2500 (M/ΔM) to discriminate the contribution of $^{18}OH^+$ ions from $^{19}F^+$ ones, but this was found to be negligible. For instrumental reasons, it was not possible to monitor the fluctuations of the primary-beam

TABLE 7. Complete EMPA data on the studied crystals (15 keV and APF corrections)

Sample	Chum HV-41 n.2		Chum HV-41 n.3		Chond HV-43 n.3		Chond HV-43 n.4		Norb HV-47 n.1	
	mean	2σ	mean	2σ	mean	2σ	mean	2σ	mean	2σ
SiO_2	38.570	0.791	38.190	1.099	34.382	0.390	34.826	0.862	29.722	0.275
B_2O_3*	0.128	0.016	0.166	0.130	0.719	0.086	0.659	0.284	0.201	0.028
TiO_2	0.626	0.252	0.411	0.155	0.046	0.032	0.044	0.054	0.083	0.027
Al_2O_3	0.005	0.019	0.047	0.071	0.009	0.022	0.022	0.028	0.000	0.000
Cr_2O_3	0.011	0.028	0.037	0.052	0.007	0.017	0.042	0.080	0.022	0.056
FeO	0.624	0.068	0.633	0.085	0.865	0.162	0.894	0.128	0.701	0.045
MnO	0.036	0.039	0.032	0.059	0.006	0.026	0.009	0.042	0.016	0.013
MgO	58.803	0.407	58.126	0.522	59.674	0.312	59.561	0.570	60.221	0.812
CaO	0.021	0.016	0.026	0.028	0.007	0.016	0.030	0.048	0.014	0.000
F	3.915	0.306	3.191	0.491	6.977	0.492	6.998	0.243	14.740	0.911
Cl	0.030	0.016	0.025	0.011	0.018	0.030	0.053	0.010	0.030	0.016
H_2O†	0.961	0.146	1.333	0.284	2.031	0.264	2.034	0.110	2.028	0.454
Total	103.728	1.384	103.060	1.059	104.741	0.276	105.172	0.748	107.779	1.063
O=F,CL	1.649	0.129	1.344	0.207	2.938	0.208	2.948	0.102	6.207	0.383
Total	102.079	1.317	101.715	1.137	101.803	0.389	102.224	0.722	101.572	1.033
Si	3.94	0.03	3.94	0.06	1.93	0.01	1.95	0.03	0.99	0.01
B	0.02	0.00	0.03	0.00	0.07	0.00	0.06	0.00	0.01	0.00
Σ tet	3.97	0.03	3.97	0.06	2.00	0.01	2.01	0.03	1.00	0.01
Ti	0.05	0.02	0.03	0.01	0.00	0.00	0.00	0.00	0.00	0.00
Al	0.00	0.00	0.01	0.01	0.00	0.00	0.01	0.01	0.01	0.00
Cr	0.00	0.00	0.00	0.00	0.00	0.00	0.00	0.00	0.00	0.00
Fe	0.05	0.01	0.05	0.01	0.04	0.01	0.04	0.01	0.02	0.00
Mn	0.00	0.00	0.00	0.01	0.00	0.00	0.00	0.00	0.00	0.00
Mg	8.96	0.08	8.95	0.10	4.99	0.03	4.96	0.07	2.98	0.01
Ca	0.00	0.00	0.00	0.00	0.00	0.00	0.00	0.00	0.00	0.00
Σ oct	9.07	0.08	9.05	0.10	5.03	0.03	5.01	0.07	3.01	0.01
F	1.27	0.09	1.04	0.17	1.24	0.09	1.24	0.04	1.55	0.10
OH	0.66	0.10	0.92	0.19	0.76	0.10	0.76	0.04	0.45	0.10
Cl	0.01	0.00	0.00	0.00	0.00	0.00	0.01	0.00	0.01	0.00
$O^{=}$	0.07	0.04	0.03	0.02	0.00	0.00	0.00	0.00	0.00	0.00
Σ CAT	13.03	0.03	13.02	0.06	7.03	0.01	7.02	0.03	4.00	0.01

* By SIMS.
† Calculated by stoichiometry.

intensity during analysis. However, as the drift of the current was <2–3% over 10 min, the average of the values measured before and after the measurement could be used as a representation of the beam intensity during analysis. Acquisition times were 80 s for ^{19}F, 10 s for ^{24}Mg, and 50 s for ^{30}Si over 10 cycles. Secondary ions were counted by an electron multiplier, which works in a pulse-counting mode and corrections were made for counting loss due to dead time (~30 nanoseconds). The analyses were done under steady state sputtering conditions, achieved after about 9 min sputtering time.

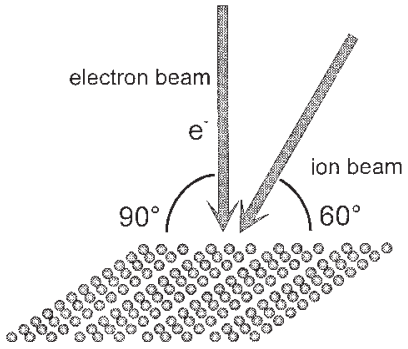

FIGURE 1. Scheme of the relationship among electron beam, ion beam, and crystal structure.

RESULTS

Structure refinement

Single-crystal refinements of the four analyzed crystals gave excellent and accurate results with very low conventional *R* factors. In all of them, the position of H atoms was located and refined, even if present in low quantity. After refinements and location of H, the residual electron density was attributed to lone pair electrons between Si and O, and between B and O. Norb HV-43 n.4 and Norb HV-47 n.1 were refined by Cámara (1997), whereas Fbor HV-43 n.2 and Fbor HV-43 n.3 by Cámara and Ottolini (2000).

Clinohumite. This is the humite-group mineral having the highest proportion of filled tetrahedral sites and therefore it possesses the structure most closely related to olivine. It displays broad OH → F substitution. However, neither OH nor F end-members are found in nature. Provided that no $Mg_{-1}R$ substitution is present (R = di-, tri-, or tetravalent cations), clinohumite unit-cell edges change with OH → F^{-} substitutions. Duffy and Greenwood (1979) modeled the variation in cell parameters for pure Mg humite-group minerals in which OH → F was the only substitution operating. Ti, Fe, and Mn entering the octahedral sites significantly change the cell-edge lengths, but the specimens analyzed here are very poor in such elements. Nevertheless, the agreement between the value calculated with the equations of Duffy and Greenwood (1979) and the refined-site scattering for fluorine in the O5 site in clinohumite is not good. The main reason for the disagreement could be ascribed to an inadequate chemical characterization of F contents in the synthesis-reac-

TABLE 7.—Extended

Norb HV-43 n.4		Norb HV-47 n.7		Fbor HV-43 n.2		Fbor HV-43 n.3		T1		T2	
mean	2σ	mean	2σ	mean	2σ	mean	2σ	mean	2σ	mean	2σ
29.490	0.694	29.392	0.400	0.207	0.658	0.037	0.147	32.322	0.687	32.069	0.418
0.183	0.038	0.333	0.122	17.690	0.016	18.240	0.280	0.000	0.000	0.000	0.000
0.089	0.039	0.067	0.058	0.007	0.018	0.017	0.027	0.000	0.000	0.000	0.000
0.013	0.022	0.006	0.022	0.035	0.051	0.014	0.057	55.919	0.445	56.172	0.330
0.015	0.051	0.000	0.000	0.010	0.028	0.022	0.070	0.000	0.000	0.000	0.000
0.682	0.051	0.549	0.030	0.169	0.067	0.158	0.106	0.030	0.050	0.040	0.043
0.035	0.079	0.039	0.026	0.006	0.020	0.000	0.000	0.000	0.000	0.000	0.000
61.111	0.101	60.984	0.351	64.186	1.799	65.075	1.178	0.006	0.018	0.001	0.006
0.033	0.043	0.033	0.043	0.094	0.287	0.101	0.387	0.007	0.018	0.006	0.017
14.463	0.640	14.321	0.946	22.381	1.231	23.296	0.759	23.006	0.952	22.558	0.489
0.023	0.012	0.027	0.012	0.036	0.016	0.030	0.028	0.000	0.000	0.000	0.000
2.212	0.372	2.267	0.399	3.590	0.488	3.398	0.352	0.000	0.000	0.000	0.000
108.348	0.501	108.017	1.166	108.411	1.944	110.388	1.109	111.289	1.370	110.846	0.730
6.090	0.269	6.031	0.398	9.425	0.518	9.810	0.320	9.69	0.401	9.50	0.206
102.257	0.727	101.986	0.821	98.986	1.544	100.578	0.983	101.60	1.109	101.35	0.588
0.97	0.01	0.97	0.01	0.01	0.02	0.00	0.00	0.97	0.01	0.97	0.01
0.01	0.00	0.02	0.00	0.97	0.01	0.98	0.01	0.00	0.00	0.00	0.00
0.98	0.01	0.99	0.01	0.97	0.03	0.98	0.01	0.97	0.01	0.97	0.01
0.00	0.00	0.00	0.00	0.00	0.00	0.00	0.00	0.00	0.00	0.00	0.00
0.00	0.00	0.00	0.00	0.00	0.00	0.00	0.00	1.98	0.02	1.99	0.01
0.00	0.00	0.00	0.00	0.00	0.00	0.00	0.00	0.00	0.00	0.00	0.00
0.02	0.02	0.00	0.00	0.00	0.00	0.00	0.00	0.00	0.01	0.00	0.00
0.00	0.00	0.00	0.00	0.01	0.00	0.00	0.00	0.00	0.00	0.00	0.00
3.01	0.03	3.01	0.02	3.03	0.06	3.02	0.03	0.00	0.00	0.00	0.00
0.00	0.00	0.00	0.00	0.00	0.01	0.00	0.01	0.00	0.00	0.00	0.00
3.03	0.03	3.03	0.02	3.04	0.05	3.03	0.02	1.98	0.02	2.00	0.01
1.51	0.08	1.50	0.09	2.24	0.11	2.29	0.07	2.18	0.08	2.15	0.04
0.49	0.08	0.50	0.09	0.76	0.11	0.71	0.07	0.00	0.00	0.00	0.00
0.00	0.00	0.00	0.00	0.00	0.00	0.00	0.00	0.00	0.00	0.00	0.00
0.00	0.00	0.00	0.00	0.00	0.00	0.00	0.00	0.00	0.00	0.00	0.00
4.02	0.01	4.02	0.01	4.01	0.03	4.01	0.02	2.95	0.02	2.96	0.01

tion products of Duffy and Greenwood (1979). Additionally, an overestimation of F on SREF could also be possible and will be discussed later.

Chondrodite. This mineral shows a higher ratio of sites with $OH_{-1}F$ substitution. Substitution of Ti, Mn, and Fe is more limited than in clinohumite. In chondrodite, Fe orders mainly in the M1 site (refined-site scattering in Table 2), which shows the highest octahedral angle variance (OAV, Robinson et al. 1971) (Table 3). The studied sample is an almost pure F end-member with a small quantity of water. The refined position of H fits well with that reported by Yamamoto (1977) for OH-chondrodite. The Duffy and Greenwood (1979) equations produce results similar to those found with clinohumite.

Topaz. The specimens analyzed here represent pure end-members. In this structure, F is concentrated in layers perpendicular to the *b* axis. No SREF analysis was performed in the T1 and T2 crystals and only cell parameters were determined.

EMPA fluorine analysis

Selecting an analyzer crystal. In the absence of a pulse-height analyzer (PHA) to account for overlapping with second-order reflections, W/Si reflectors are inadequate for the analysis of matrices with up to 60 wt% MgO or high Al_2O_3, such as those investigated in this study. Considering that P is not present in our minerals, in spite of the low counting rates, we decided to measure the F$K\alpha$ peak with a RAP crystal [Rubidium Acid Phthalate; $2d = 26.12$ Å; Bragg diffraction (100)].

Standards. We tested common fluorine standards such as Durango apatite, fluorite, synthetic LiF, and cryolite, none of which is a silicate matrix. Apatite presents serious problems of beam-damage and should be used with an accurate control of beam exposure and crystal orientation (Stormer et al. 1993). Cryolite contains Na and will present problems related to diffusion of this element. Fluorite can show decay of counting rates during beam exposure but it is always less dramatic than that for apatite (Stormer et al. 1993). We have performed beam-exposure damage test on apatite, fluorite, and on T1 and T2 topaz, confirming the results of Stormer et al. (1993).

Beam characteristics. The beam energy is also a fundamental parameter when dealing with accurate light-element analysis. By increasing the beam energy, X-ray counts increase but X-rays are produced deeper in the sample, thus creating problems related to absorption of the emitted radiation. The typical beam energy for light-element analysis ranges between 7 and 15 keV. We have made analyses under both conditions to check for the dependence of experimental data on the electron-beam energy. The peak to background ratios were much higher at 7 keV than 15 keV, and this was more evident in samples with low F concentrations, i.e., clinohumite and chondrodite. Counting rates are also increased by increasing beam current. However, raising the beam current to high levels causes awkward experimental conditions (Bastin and Heijligers 1991) such as instability of the beam current. We also checked different beam currents and chose 20 nA as a good compromise between counting-rates and precision under stable experimental conditions.

Another important parameter is the beam diameter. For

standard analytical procedures, a typical beam diameter of 1–2 micrometers is used to enhance its probe characteristics. However, such a focused beam enhances beam damage in the irradiated area and diffusion easily takes place. The apatite and fluorite standards showed counting-rate decay in the first 100 s with a beam diameter of 3 μm (15 keV and 20 nA); it was less severe in fluorite. However, no apparent decay was detected in any of them with a beam diameter of 30 μm, even with longer exposures. For this reason, we selected a beam diameter of 30 μm in the present study.

Absorption corrections. Available mass-absorption coefficients for F seem to work well even at different accelerating voltages. We used the $\phi(\rho z)$ correction included in the quantitative microprobe software PROBE, version 3.63 (Donovan and Rivers 1990), which runs the ARL-SEMQ microprobe at the University of Modena. We have found very significant differences by taking into account unanalyzed elements (such as B in fluoborite) in the correction procedures. This is due to the fact that the stoichiometric amount of boron is 18.47 wt% (as B_2O_3) in fluoborite. Specifying this quantity of B in the data-correction program causes a change in the F-estimated concentration by more than 7% (relative). Another problem with F is the absorption correction in high-F matrices since oxygen (unanalyzed) is estimated incorrectly by stoichiometry unless the oxygen-equivalent of F is subtracted from the calculated stoichiometric oxygen.

Peak shifts and peak shapes. To calculate our APFs and check for their dependence on crystal orientation and accelerating voltage, we performed wavelength scans of 100 steps at 6 seconds/step in the range of 0.6 Å around the F-peak position. The sample current was 20 nA and the beam diameter was 30 μm. Wavelength scans were collected at 7 keV and 15 keV on a CaF_2 standard, humite-group minerals, fluoborite and topaz samples. Reproducibility tests were made on CaF_2 under both analytical conditions. Wavelength-scan data were processed by Jandels *PeakFit* program, performing on each scan an automated FFT, Gaussian deconvolution procedure, a linear baseline subtraction, and the Gaussian amplitude fitting. The peak-height/peak-area ratio was calculated for each scan. These values, normalized to the peak-height/peak-area ratio measured on CaF_2 are the APFs reported in Table 6a and 6b. The fitted peaks correspond to the $FK\alpha_{1,2}$, $FK\alpha_{3,4}$, and $FK\alpha_{5,6}$ at higher energies and an unresolved fourth peak at lower energies, but only for the topaz. We considered all of these peaks in the integration for the calculation of APFs. Since we cannot easily resolve them with RAP for the topaz, the integrated areas are no longer equivalent if we do not integrate them all together.

Changing the accelerating voltage and the crystal orientation, peak shifts (~0.02 Å) are within the experimental error whereas slight peak-shape changes can be observed for most of the studied crystals, resulting in only rather limited APF variations. Fluoborite shows a slight peak shift, with a significant variation in intensity, increasing from sample Fbor HV-43 n.2 (*c* axis parallel to the electron beam) to Fbor HV-43 n.3 (*c* axis perpendicular to the electron beam). As previously noted in other studies (Solberg 1982; Fialin et al. 1993), the topaz peaks are wide and unresolved. The modeled peaks change in shape, amplitude, and full-width at half-maximum (FWHM) as the angle between the *c* axis and the detector changes. This had been found previously for B by Bastin and Heijliger (1991).

We decided to test the effect of rotation changing the angle between crystal and detector, and observed that in topaz the APFs increase and decrease as the crystal is spun (APF range of variation: 1.17–1.70 in T2). Minor variations were found in Norb HV-47 n.7 and Fbor HV-43 n.2 (APFs range 1.08–1.22). Therefore, we do not envision a systematic peak behavior for fluoborite and humite-group crystals with respect to fluorite. In topaz, our APF-mean values are very similar to those reported by Fialin et al. (1993) [1.5 using fluorite as a standard, compared with 1.47 of Fialin et al. (1993) using LiF].

The differences between the APFs calculated at 7 keV (Table 6a) for the crystals with the plane of maximum density of F atoms perpendicular to the electron beam and those with general orientation are significant ($> 2\sigma$) only for chondrodite. In the other cases, the discrepancies are within the analytical errors.

At 7 keV we only analyzed F because the accelerating voltage is too low to get accurate and reproducible data for higher-Z elements (e.g., Si, Mg) to be used as internal reference elements in SIMS measurements. In Table 7 we report the data obtained at 15 keV for major-element analyses, F corrected for APFs, and H_2O calculated by stoichiometry. Boron contents were obtained by SIMS according to the procedure outlined in Ottolini et al. (1993). We find a fairly good agreement between EMPA and SREF in terms of electron per site (~2% relative). Nevertheless, SREF F-concentrations appear to be systematically higher, which we will discuss later.

SIMS fluorine analysis

We followed an empirical approach to quantification, with Mg and Si selected, in turn, as the matrix-reference element, and F concentrations determined by EMPA. For SIMS we utilized the same samples and mounts as for EMPA.

Four different data sets were then obtained for F concentrations from EMP analyses at 15 and 7 keV without and with APF corrections; for major-element concentrations, we relied on those measured at 15 keV. This should provide us with a presumably lower standard deviation for major-element data. Two sets of working curves were then obtained and compared.

Reference element: Mg

15 keV (no APFs). A linear fit (regression coefficient $R^2 = 0.96$), i.e., ion-intensity ratio F^+/Mg^+ vs. F(at)/Mg(at) [where F^+ and Mg^+ represent their secondary ion signals corrected for isotopic abundance, and (at) represents their relative atomic concentration (in percent)] was obtained for all samples (Fig. 2a); the error bars represent $\pm 2\sigma$. The agreement between the experimental data and fitted line was generally within or comparable to the experimental error. In only a few cases was the discrepancy higher. Norb HV-43 n.4 showed the higher IY (= 0.021) and does not lie on the line. In contrast, the two fluoborite crystals (filled circles in Fig. 2a) showed the lower IYs, the major discrepancy from the regression line being presented by Fbor HV-43 n.3 with its *c* axis perpendicular to the electron beam (60° to the ion beam); its IY(F/Mg) is 0.016.

15 keV (with APFs). By applying APF corrections, the regression coefficient of the curve does not appreciably change ($R^2 = 0.97$) whereas its angular coefficient [representing IY(F/Mg)] decreases by ~11% rel. (Fig. 2b). Clinohumite and chondrodite

data lie on the line. The higher discrepancies (≤11%) are shown by Norb HV-43 n.4 and Norb HV-47 n.7; their IYs are higher than those predicted by the working line. The SIMS results are within the analytical error for Norb HV-47 n.1. The IY in fluoborite crystals in both orientations is still lower than for other samples (≤8% respect to the line).

7keV (no APFs). If we use only one working line for all experimental data, the regression coefficient is the same as that for EMPA-15 keV with APF corrections ($R^2 = 0.97$). The major discrepancies are presented by Norb HV-47 n.7 (*a* axis at 35° to the electron beam and *b* axis at 74° to the electron beam) and Chond HV-43 n.3 (*a* axis at 56° to the electron beam and *b* axis at 53° to the electron beam), 18% and 14%, respectively, which are higher than analytical uncertainty. Fbor HV-43 n.2 (*c* axis parallel to electron beam) shows an IY lower (by 9% relative) than that predicted by the line.

In general, the "disoriented" samples, i.e., samples mounted in a general orientation to the electron beam (open circles in Fig. 2c) show an ion yield higher than that of the "oriented" ones (open triangles in Fig. 2c) with the relative difference being ~14%. This difference holds for humite-group minerals, suggesting that we should use these two lines (Fig. 2c). Indeed, the correlation is very good ($R^2 = 1$) for both lines, which define two different trends as a function of orientation. Interestingly, Norb HV-43 n.4 and Norb HV-47 n.1, which differ by ~10° relative, show a small variation of their IYs around a value that is typical for "oriented" samples.

The fluoborite crystals show a lower IY, the lowest pertaining to Fbor HV-43 n.2. The maximum difference among all these ion yields is ~25%. When working under these experimental conditions, the present results must be taken into account because the

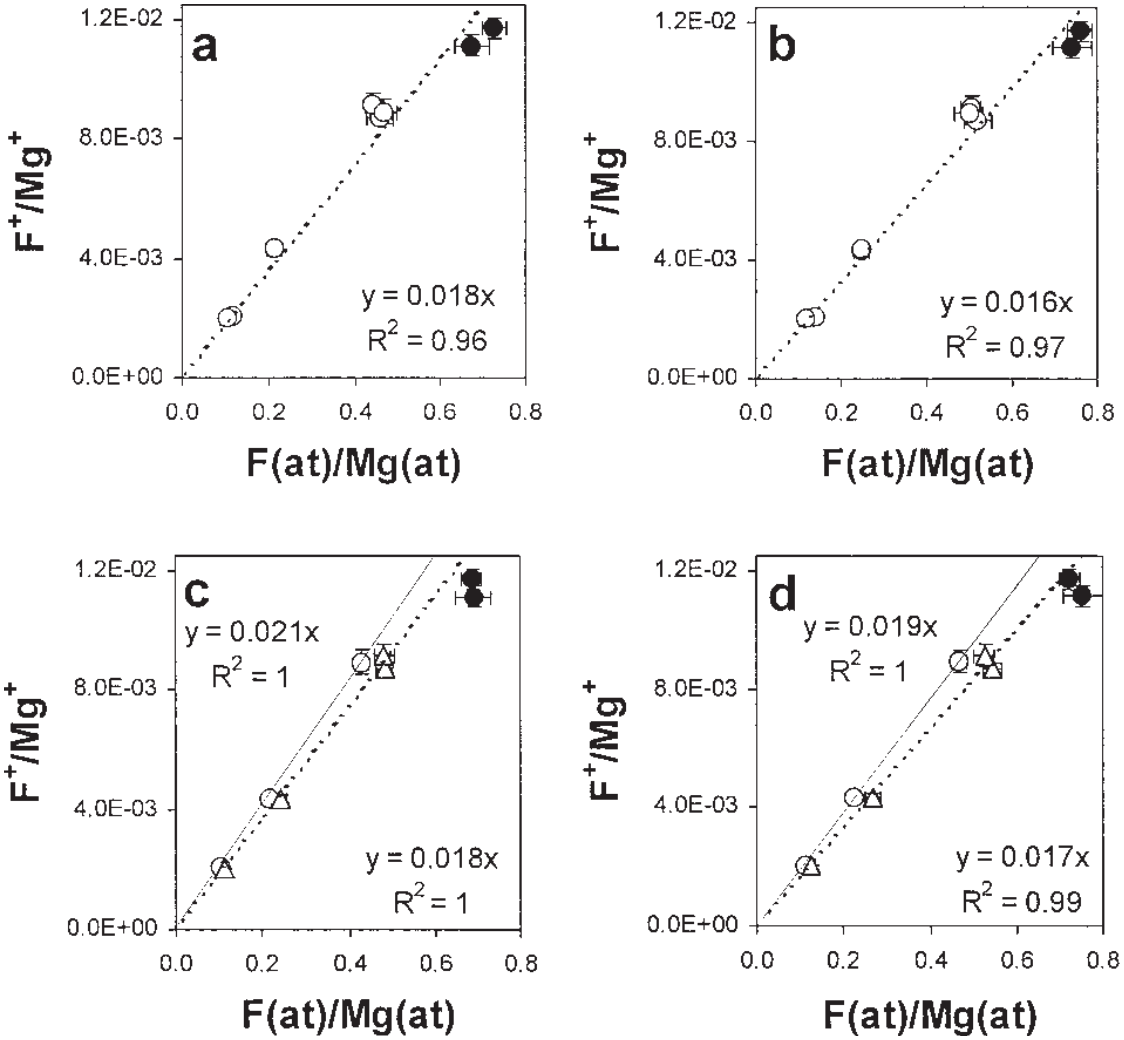

FIGURE 2. Working curves F(Mg), obtained by plotting ion intensity ratio F^+/Mg^+ vs. at concentration ratio F(at)/Mg(at). Concentrations from EMP analyses obtained at 15 keV without (**a**) and with (**b**) APF correction; and at 7 keV without (**c**) and with (**d**) APF correction. Symbols: open circles = all humite-group samples (in **a** and **b**) and "disoriented" humite-group samples (in **c** and **d**); open triangles = "oriented" humite-group samples; filled circles = fluoborite samples.

IY derived from a "disoriented" norbergite (for example, Norb HV-47 n.7), which was used as an F-reference sample to quantify an "unknown" fluoborite, could result in up to ~25% inaccuracy, depending on matrix effects.

7keV (with APFs). Correcting the F content by applying APFs results in a decrease of the IY(F/Mg) by ~10% relative for "disoriented" samples and ~6% relative for "oriented" ones (Fig. 2d; symbols as in Fig. 2c), with $R^2 \cong 1$ for both lines. These data suggest that residual matrix effects related to the different chemical compositions within a selected orientation (for example, "disoriented" samples) are of the same amount, with differences among humite-group minerals being within analytical error. Depending on orientation, the results define two IYs, differing by ~12%; in the most unfavorable cases, the difference among all IYs, including those of fluoborite crystals, can be up to ~27%.

The effects related to crystal orientation therefore seem to play a previously unconsidered role. The two fluoborite crystals show a behavior similar to that of "oriented" minerals of the humite-group. Interestingly, with the application of APFs, the IY of Fbor HV-43 n.3 (*c* axis perpendicular to the electron beam), is the same as that of "oriented" crystals: matrix effects (if any) are of the same order. The IY(F/Mg) of Fbor HV-43 n.2, is still lower, however.

Reference element: Si

For comparison, working curves F^+/Si^+ vs. F(at)/Si(at) constructed with respect to Si are reported in Figure 3. The EMP data for humite-group minerals and for T1 and T2 (electron beam parallel to *b* axis and parallel to *c* axis, respectively) have been studied in the four cases as before: 15 and 7 keV, without and with APF corrections.

15 keV. F^+/Si^+ ion signals correlate linearly with their respective concentration ratios, F(at)/Si(at) (Fig. 3a; no APF corrections). All humite-group data lie on the line within the analytical error ($R^2 = 0.99$; IY = 0.026). The IY(F/Si) in T1 and T2 is the same and is ~40% lower. SiO_2 content is similar in all these samples. The ionization behavior of F/Si in topaz does not seem to be particularly sensitive to the different crystal orientation of the grains.

Applying APF corrections, the IY(F/Si) for humite-group minerals and topaz changes by ~11% and 26%, respectively. The whole change results in ~50% difference between the two sets of Mg- and Al-basis samples (Fig. 3b). The regression coefficient R^2 is equal to 1.

7 keV. Working with 7 keV (no APF corrections) (Fig. 3c) the agreement between the IY for humite-group minerals and that for topaz is within 39% relative, ($R^2 = 0.99$; IY = 0.026). Norb HV-47 n.7 presents the higher discrepancy (8%) and does not lie on the line; Norb HV-47 n.1 shows a lower IY, with a discrepancy that is slightly higher than the analytical uncertainty. T1 and T2 exhibit similar IYs.

The application of APF corrections increases the discrepancy between the IY(F/Si) in Mg- and Al-basis minerals. This allows us to propose two working curves for "oriented" as well as "disoriented" samples with $R^2 = 0.99$ and $R^2 = 1$, respectively (Fig. 3d), whose slopes differ by ~12%.

The different fluorine peak-shape in topaz compared with that of humite-group minerals, and the impossibility of discriminating among the different peak components for this matrix, probably do not allow us to apply an APF correction that is equivalent for all these samples. Bonding between fluorine and major constituents in the matrix is quite different: of ionic type for humite-group minerals, but of covalent type in topaz. The bonding plays a decisive role in this matrix, and also in the acquisition of EMP spectra. As already noted by Fialin et al. (1993), the F$K\alpha$ band emitted by a highly ionic compound (i.e., LiF) and by a topaz, in which the ionic nature of the F-Al bond is less pronounced, is different. Following Fialin et al. (1993), a first indication of the "less-ionic structure" of the emitted F$K\alpha$ band from topaz is the reduction of the satellite emission, which can be deduced from the obvious loss in intensity of $K\alpha_{5,6}$ band (the $K\alpha_{3,4}$ doublet at 3.4 eV from the peak is not resolved and appears as a shoulder of $K\alpha_{1,2}$). The contribution of filled *p*-character states due to the mixing of F 2*p* and Al 3*sp* valence states to form the covalent F-Al bond is without doubt responsible for the low-energy satellite that appears as a shoulder at ~–3 eV from the main peak of the topaz (Fialin et al. 1993).

One additional difference for topaz is the fact that APF corrections are very sensitive to the sample-detector relative orientation. In our case we used an APF of 1.5 as the average of the values 1.17–1.70. In fact, for a more-accurate correction, the APFs should be applied to the actual measurement conditions for each sample position. Therefore, these results are only indicative of what can happen under "routine" EMP analysis. The estimation of the actual amount of matrix effects between Mg-enriched samples and topaz should take into account how critical the influence of APF corrections is for EMP analyses on topaz.

In our opinion the difference in the IY(F/Si) between topaz and humite-group minerals with the above specifications can be ascribed to both different chemical compositions and structures. In humite-group minerals, silicon is bonded to four oxygen atoms in tetrahedral coordination with a highly covalent-character to the bonding. Magnesium is always in octahedral coordination with a highly ionic bonding and can be bonded to a different number of F atoms, depending on the specific structure.

A comparison between the ion signals of F and Si in norbergite and topaz allowed us to calculate an absolute IY[F^+/F(at)] that is higher by a factor of ~3.7 in the former (with F ≈ 14 wt%) than in the latter (with F ≈ 20 wt%). In humite-group minerals, the Si ionization increases as well, although to a lesser extent: the absolute IY[Si^+/Si(at)] is higher by a factor of ~1.5 in norbergite (29.7 wt% SiO_2) than in topaz (32.1 wt% SiO_2), and the overall result is an increased IY(F/Si) in humite-group minerals. These results were obtained in the same analytical runs, with an accurate and constant control of focusing conditions and primary-beam current-intensity and their reproducibility was checked on different analytical sessions over a three-month span.

In our opinion, the enhanced ion yield for F in humite-group minerals could be related first to a higher F-sputter yield (F-sputtered atoms/O^- primary ions) due to the lower bond dissociation energy of F-Mg diatomic molecules (461.9 D^0_{298}/kJ mol^{-1}) (Kerr 1989) than that of Al-F molecules in topaz (663.6 D^0_{298}/kJ mol^{-1}) (Kerr 1989). EMPA and SIMS results allow us to conclude that the superposition between atomic shells involved

in the Al-F covalent bonding is quite high and therefore the resulting bonding is rather strong. This could justify the experimental evidence of a lower IY(F/Si) in silicates in which F is characterized by a covalent bonding (Al-F).

Using silicon as the internal standard for 15 keV EMP analysis (with or without APF correction), it is possible to get only one working curve for humite-group minerals with a regression coefficient close to 1. This implies that the overall matrix effects—related to structure, crystal orientation, and chemical composition—within this set of samples are rather limited. Considering the uncertainty of our previous working curve for F (±20% rel.) (Ottolini et al. 1994), based mainly on Al-enriched samples, the ion yield variation due to residual matrix effects between Mg-rich and Al-rich silicates may be estimated to be on the order of 40% relative.

Comparison of EMPA-SIMS-SREF results

In Table 8 we have reported the final data relative to all EMP analyses, obtained at 15 keV and corrected for APFs, compared with SIMS and SREF results. SIMS data are calculated with, in turn, Mg (top) and Si (bottom) as the matrix-reference element. They are plotted in Figure 4.

Let us first consider EMPA vs. SREF (Fig. 4a). The discrepancy is within ~11% for most samples (~15% for Chum HV-41 n.2). The regression coefficient R^2 is 1. The F content is systematically lower for EMP data (except for Chum HV-41 n.2). This result can be understood in terms of absorption of F$K\alpha$ X-ray radiation in the sample or an overestimation of the site occupancies during the refinement of crystal data. In the present conditions (15 keV, with APFs), the effect of crystal orientation on EMP analyses was found to be typically within the uncertainty of analysis (2σ) (see Table 6b), whereas the difference in F data at 7 keV (with or without APF correction) between "disoriented"

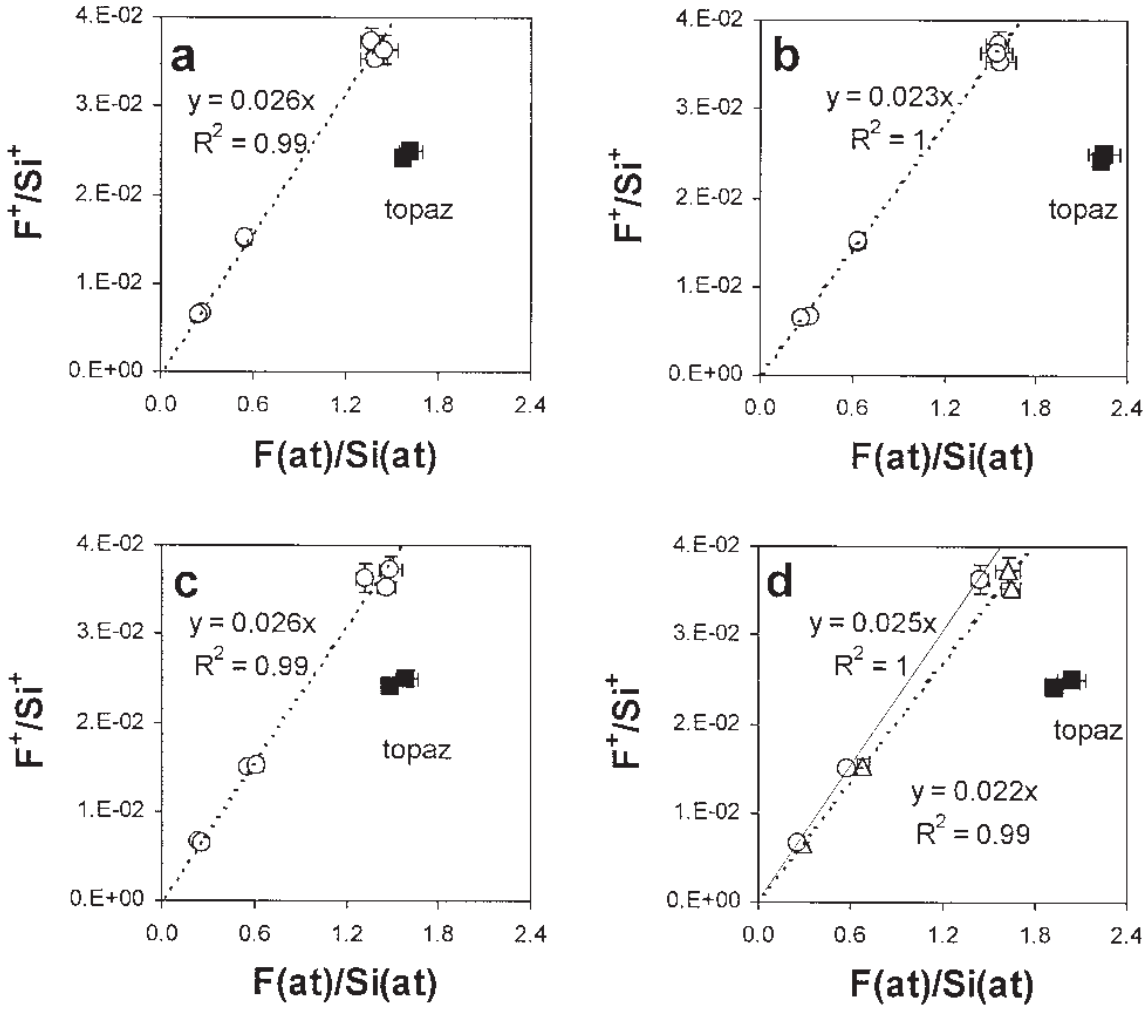

FIGURE 3. Working curves F(Si), obtained by plotting ion intensity ratio F^+/Si^+ vs. at concentration ratio F(at)/Si(at). Concentrations from EMPA obtained at 15 keV without (**a**) and with (**b**) APF correction; and at 7 keV without (**c**) and with (**d**) APF correction. Symbols: open circles = all humite-group samples (in Fig. 3a, 3b, and 3c) and "disoriented" humite-group minerals (in Fig. 3d); open triangles = "oriented" humite-group samples; filled squares = topaz samples.

and "oriented" samples was found to be significant (> 2σ) in some cases (see Table 6a).

Looking at the SIMS vs. SREF correlation using Mg as the reference element (Fig. 4b), we see that the SIMS data inherit the characteristics of EMP analyses that represent here the reference for SIMS. The correlation index is a little lower ($R^2 = 0.97$). The plot shows the presence of further matrix effects related to sputtering/ionization phenomena, mostly evident in F-enriched minerals, such as fluoborite, which does not contain Si, but has high contents of F and B. In such a case, SIMS data are lower than SREF estimations; the lowest F value (~17% rel.) being represented by sample Fbor HV-43 n.2.

EMPA vs. SREF data (Fig. 4c) show a correlation similar to that in Figure 4a, i.e., $R^2 = 0.99$; y = 0.93x. In the latter plot we have simply excluded data for fluoborite. The correlation improves ($R^2 = 1$) considering SIMS vs. SREF, with Si as the matrix element (Fig. 4d). In such a case, the discrepancy is within 11% relative, similar in most cases to the analytical uncertainty. This choice results also in the exclusion of fluoborite that does not contain silicon, which presents the major SIMS matrix effects among the investigated Mg-enriched samples.

The systematically higher F-content estimations by SREF could be attributed to a certain degree of positional disorder between the location of F and O atoms in the same site. This positional disorder results, during the refinement, in a higher atomic displacement parameter (a.d.p.) of the site where the $O_{-1}F$ exchange takes place (nearly 50% higher than for the rest of the anions, Table 2), which turns into a higher estimated F-content because of the high correlation between occupancy and a.d.p.

Another possible cause of error of the F-content could be due to the fact that both light elements (F and O) differ only in their scattering curves at very low resolution; small errors in the correct determination of intensities can introduce easily a ~10% relative error in the determination of F site occupancies.

Recommended analytical protocol

F analysis by EMP can be accurate within experimental error if a preliminary study of APFs, peak shifts, and beam damage to standards and samples are performed. In the analysis of F we found it advisable to use large diameter beam (~30 μm), intermediate accelerating voltage (15 kV), and low to medium beam-current (20–30 nA). On-peak counting times of 30 seconds seem to work well in most of the studied samples. Close attention to the matrix and ZAF corrections is desirable because the absorption factors and the Z corrections involved can be very high (up to three times the correction required for other elements). For F analysis, it is necessary to subtract the equivalent quantity of oxygen before performing the ZAF corrections.

(1) When accurate control of shift and peak-position is performed and a careful integration and calculation of APFs is done, it is possible to obtain EMP data in agreement with SREF data within typically 11% relative.

(2) Norbergite is proposed as a very suitable standard for the EMP analysis of F in silicates. It displays very limited peak shift and shape changes with orientation, and is stable under the electron beam. Other humite-group minerals could also be suitable with the exception of clinohumite in which the F content is low and thus easily affected by instabilities during data acquisition with EMP. Due to the important analytical difficulties discussed above, it is not possible to obtain reliable F analyses in topaz unless an accurate control of its relative orientation with respect to the analyzer crystal can be taken into account and necessary APFs figured out. Therefore we strongly discourage the use of topaz as standard for fluorine in EMP analysis. Independently of the chosen F standard, the corresponding APFs must be calculated for all the F-bearing minerals to be analyzed.

(3) Considering the relative ionization behavior of F, Si is a suitable internal reference-element. A SIMS working curve F(Si) ($R^2 = 1$) can be obtained for all humite-group minerals with 15 keV EMPA data. This result implies that the overall matrix effects—related to structure, crystal orientation, and chemical composition—within this set of samples are rather low.

Table 8. Comparison among SREF, SIMS and EMP F-data for the studied crystals

Sample	Reference	SREF (F wt%)	st. dev. (2σ)	SIMS F wt%	st. dev (2σ)	EMPA F wt%	st. dev. (2σ)	d (SREF-SIMS) (%)	d (SREF-EMPA) (%)
	MgO wt%								
Norb HV-47 n.1	60.22	15.61	0.94	15.16	0.32	14.74	0.91	2.9	5.6
Norb HV-43 n.4	61.11	15.61	0.94	16.13	0.70	14.46	0.64	–3.3	7.4
Norb HV-47 n.7	60.98	15.61	0.94	15.74	0.69	14.32	0.95	–0.8	8.3
Chum HV-41 n.2	58.80	3.42	0.21	3.52	0.08	3.92	0.31	–2.9	–14.6
Chum HV-41 n.3	58.13	3.42	0.21	3.42	0.03	3.19	0.49	0.0	6.7
Chond HV-43 n.3	59.67	7.83	0.47	7.48	0.36	6.98	0.49	4.5	10.9
Chond HV-43 n.4	59.56	7.83	0.47	7.51	0.22	7.00	0.24	4.1	10.6
Fbor HV-43 n.3	65.08	24.84	1.49	22.06	0.76	23.30	0.76	11.2	6.2
Fbor HV-43 n.2	64.19	24.84	1.49	20.67	0.88	22.38	1.23	16.8	9.9
	SiO_2 wt%								
Norb HV-47 n.1	29.72	15.61	0.94	14.16	0.13	14.74	0.91	9.3	5.6
Norb HV-43 n.4	29.49	15.61	0.94	14.91	0.66	14.46	0.64	4.5	7.4
Norb HV-47 n.7	29.39	15.61	0.94	14.45	0.68	14.32	0.95	7.4	8.3
Chum HV-41 n.2	38.57	3.42	0.21	3.47	0.12	3.92	0.31	–1.5	–14.6
Chum HV-41 n.3	38.19	3.42	0.21	3.36	0.18	3.19	0.49	1.8	6.7
Chond HV-43 n.3	34.38	7.83	0.47	6.93	0.28	6.98	0.49	11.5	10.9
Chond HV-43 n.4	34.83	7.83	0.47	7.21	0.36	7.00	0.24	7.9	10.6
T1	32.32			10.95	0.37	23.01	0.95		
T2	32.07			10.46	0.34	22.56	0.49		

Note: EMPA data (corrected for APFs) are relative to 15 keV. SIMS values were quantified respect to Mg (top) and Si (bottom) selected as the internal standard.

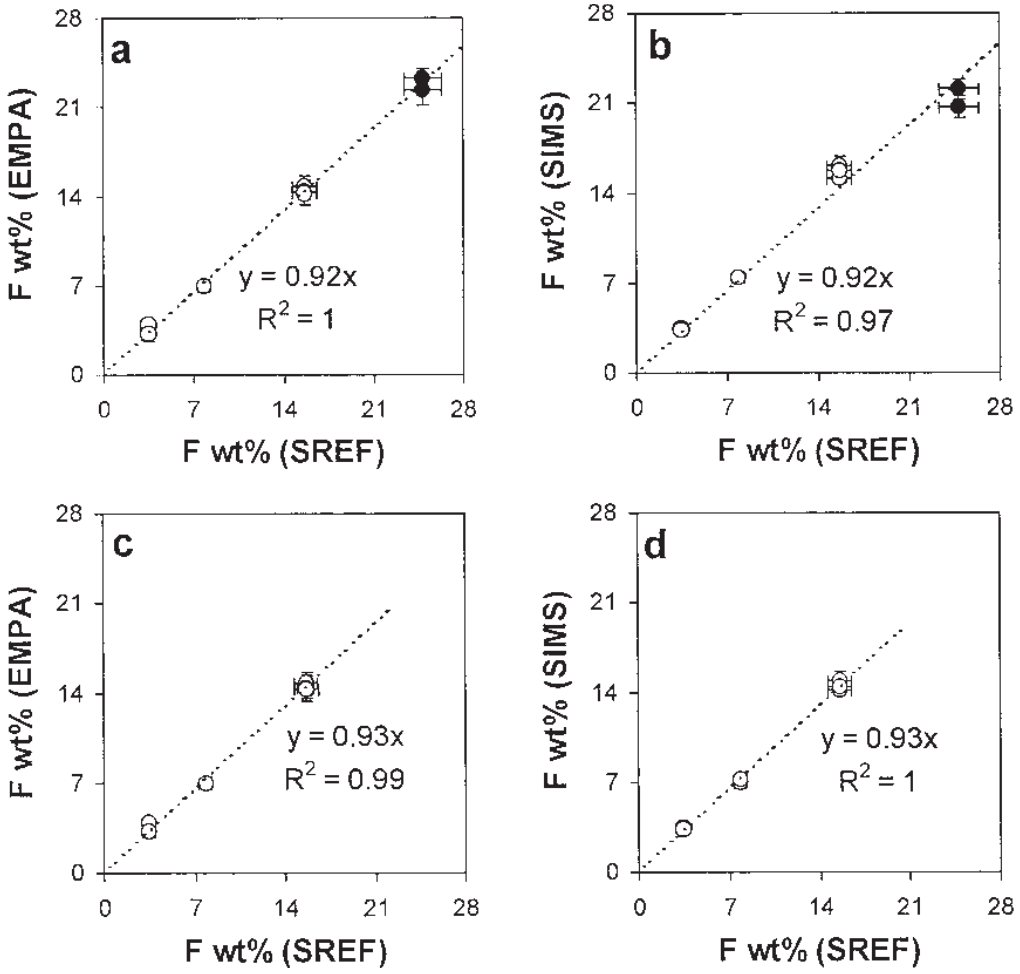

FIGURE 4. Comparison between wt% F (EMPA) and wt% F (SREF) values (**a**) fluoborite included and (**c**) fluoborite not included. Comparison between wt% F (SIMS) and wt% F (SREF) calculated with respect to (**b**) Mg (EMP at 15 keV with APFs) and (**d**) Si (EMP at 15keV with

(4) SIMS measurements in humite-group minerals do not introduce significant matrix effects with respect to EMP analysis and can provide a close agreement with SREF crystallographic results. In analyzing fluoborite, additional SIMS matrix effects must be taken into account: in the most unfavorable cases, the difference in IY(F/Mg) between "disoriented" humite-group minerals and "oriented" fluoborite can reach ~27%.

(5) For topaz, we suggest the use of APF corrections in EMP analyses and, for SIMS quantification, the use of a topaz standard previously characterized by bulk as well as microanalytical techniques. An accelerating voltage of 15 kV is a good choice for EMP analysis of topaz. If the F contents derived from SIMS, EMP, or SREF analyses are to be used in the estimation of liquid-solid distribution coefficients for accurate determination of activity-composition relationships in metamorphic, metasomatic, or igneous reactions, careful attention must be paid to making a reliable estimation of that element, or a complementary H-content estimation by SIMS is advisable.

(6) SREF is suspected to be overestimating F contents for reasons that are difficult to attribute in a simple way to standard SREF analyses. Geometrical constraints (such as correlation between single cation-F bond distances, or cell parameters, and independently estimated F content) are useful to double-check the consistency of data. Unfortunately few complete data sets are available to perform such correlation with different mineral groups and more crystal-chemical work is required.

ACKNOWLEDGMENTS

The authors thank J. Currás (University of Granada, Spain), who kindly provided the samples of humite-group minerals and fluoborite. Fruitful advice was obtained from T. Solberg, H. Heijligers, and M. Fialin in researching bibliography in electron microprobe analysis. J.J. Donovan is particularly acknowledged for suggesting the APF-correction procedure, and in EMP-data treatment. The authors are indebted to D. Dickie for improving the English version of the manuscript. R. Gastoni is thanked for skillful sample preparation on the EMPA-SIMS mountings and M. Palenzona for ion-probe maintenance. Sincere thanks to R.F. Dymek, J.R. Hinthorne, and R.J. Tracy for their careful revisions that greatly improved the manuscript.

The Consiglio Nazionale delle Ricerche is acknowledged for financing the electron microprobe laboratory in the University of Modena, and the ion microprobe at CSCC (Pavia), whose facilities were used in the present work. Financial support to F.C. from

a FPU research fellowship of the Spanish M.E.C. is acknowledged.

REFERENCES CITED

Bastin, G.F. and Heijligers, H.J.M. (1986a) Quantitative electron probe microanalysis of carbon in binary carbides. Parts I and II. X-ray Spectroscopy, 15, 135–150.
——(1986b) Recent developments in EMPA of very light elements. In J.D. Brown and R.H. Packwood, Eds., 11th Int. Congress on X–ray optics and Microanalysis, p. 257–261. ICXOM, London, Ontario.
———(1986c) Quantitative electron probe microanalysis of boron in some binary borides. In A.D. Romig, Jr. and W.F. Chambers, Eds., Microbeam Analysis, p. 285–288. San Francisco Press, Inc., California.
———(1986d) Quantitative electron probe microanalysis of boron in binary borides. Internal Report Eindhoven University of Technology, Eindhoven, The Netherlands.
———(1988) Quantitative electron probe microanalysis of nitrogen. Internal Report of Eindhoven University of Technology, Eindhoven, The Netherlands.
——(1989) Quantitative EMPA of oxygen. In P.E. Russell, Ed., Microbeam Analysis, p. 207–210. San Francisco Press, Inc., California.
———(1991) Quantitative electron probe microanalysis of ultra-light elements (boron-oxygen). In K.F.J. Heinrich and D.E. Newbury, Eds., Electron Probe Quantification, p. 145–161. Plenum Press, New York, U.S.A.
Blessing, R.H., Coppens, P., and Becker, P. (1974) Computer analysis of step scanned X-ray data. Journal of Applied Crystallography, 7, 488–492.
Busing, W.R., Martin, K.O., and Levy, H.A. (1962) ORFLS, a Fortran crystallographic least-squares program. Oak Ridge National Laboratory, Report ORNL-TM-305.
Cámara, F. (1997) New data on the structure of norbergite: hydrogen location by X-ray diffraction. Canadian Mineralogist, 35, 1523–1530.
Cámara, F. and Ottolini, L. (2000) New data on the fluoborite crystal-chemistry by means of SREF, SIMS, and EMP analysis. American Mineralogist, 85, 103–107.
Donovan, J.J. and Rivers, M.L. (1990) PRSUPR—A PC Based Automation and Analysis Software Package for Wavelength-Dispersive Electron-Beam Microanalysis. Microbeam Analysis, p. 66–68.
Duffy, C.J. and Greenwood, H.J. (1979) Phase equilibria in the system MgO-MgF_2-SiO_2-H_2O. American Mineralogist, 64, 1156–1174.
Fialin, M., Hénoc, J., and Remond, G. (1993) A survey of Electron Microprobe Microanalysis using soft radiations: difficulties and presentation of a new computer program for wavelength dispersive spectrometry. Scanning Microscopy Supplement, 7, 153–166.
Gibbs, G.V. and Ribbe, P.H. (1969) The crystal structures of the humite minerals. I. Norbergite. American Mineralogist, 54, 376–390.
Gibbs, G.V., Ribbe, P.H., and Anderson, C.P. (1970) The crystal structures of the humite minerals. II. Chondrodite. American Mineralogist, 55, 1182–1194.
Goldstein, J.J., Newbury, D.E., Echlin, P., Joy, D.C., Romig, A.D., Lyman, C.E., Fiori, C., and Lifshin, E. (1992) Scanning Electron Microscopy and X-ray Microanalysis (2nd ed.) Plenum Press, New York, U.S.A.
Hawthorne, F.C., Ungaretti, L., and Oberti, R. (1995) Site populations in minerals: terminology and presentation of results of crystal-structure refinement. Canadian Mineralogist, 33, 907–911.
Hervig, R.L., Kortemeier, W.T., and Burt, D.M. (1987) Ion microprobe analyses of Li and B in topaz from different environments. American Mineralogist, 72, 392–396.
Hinthorne, J.R. and Andersen, C.A. (1975) Microanalysis for fluorine and hydrogen in silicates with the ion microprobe mass analyzer. American Mineralogist, 60, 143–147.
Ihinger, P.D., Hervig, R.L., and McMillan, P.F. (1994) Analytical Methods for Volatiles in Glasses. In Mineralogical Society of America Reviews in Mineralogy, 30, 67–121.
Jones, A.P. and Smith, J.V. (1984) Ion probe analysis of H, Li, B, F and Ba in micas with additional data for metamorphic amphibole, scapolite and pyroxene. Neues Jahrbuch für Mineralogie Monatshefte, June 1984, 5, 228–240.
Jones, N.W., Ribbe, P.H., and Gibbs, G.V. (1969) Crystal chemistry of the humite minerals. American Mineralogist, 54, 391–411.
Kerr, J.A. (1989) Strengths of chemical bonds, F-174, F-176. Handbook of Chemistry ad Physics 69th Ed., CRC Press Inc., New York, USA.
Kovalenko, V.I., Hervig, R.L., and Sheridan, M.F. (1988) Ion-microprobe analyses of trace elements in anorthoclase, hedenbergite, aenigmatite, quartz, apatite, and glass in pantellerite: Evidence for high water contents in pantellerite melt. American Mineralogist, 73, 1038–1045.
Lehmann, M.S. and Larsen, F.K. (1974) A method for location of the peaks in step-scan-measured Bragg reflections. Acta Crystallographica, A30, 580–584.
Messerschmidt, A. and Pflugrath, J.W. (1987) Crystal orientation and X-ray pattern prediction routines for area-detector diffractometer systems in macromolecular crystallography. Journal of Applied Crystallography, 20, 306–315.
Moore, P.B. and Araki, T. (1974) Pinakiolite, $Mg_2Mn^{3+}O_2[BO_3]$; warwickite $Mg(Mg_{0.5}Ti_{0.5})O[BO_3]$; wightmanite $Mg_5O(OH)_5[BO_3]nH_2O$: crystal chemistry of complex 3 Å wallpaper structures. American Mineralogist, 59, 985–1004.
North, A.C.T., Phillips, D.C., and Mathews, F.S. (1968) A semi-empirical method of absorption correction. Acta Crystallographica, A24, 351–359.
Ottolini, L., Bottazzi, P., and Vannucci, R. (1993) Quantification of lithium, beryllium and boron in silicates by Secondary Ion Mass Spectrometry using Conventional Energy Filtering. Analytical Chemistry, 65, 1960–1968.
Ottolini, L., Bottazzi, P., and Zanetti, A. (1994) Quantitative analysis of hydrogen, fluorine and chlorine in silicates using energy filtering. In A. Benninghoven, Y. Nihei, R. Shimizu, H.W. Werner, Eds., SIMS IX Proceedings, p. 191–194. Wiley, Chichester, U.K.
Penfield, S.L. and Howe, W.T.H. (1894) On the chemical composition of chondrodite, humite and clinohumite. American Journal of Science, Series 3, 47, 188–206.
Potts, P.J. and Tindle, A.G. (1989) Analytical characteristics of a multilayer dispersion element ($2d$ = 60 Å) in the determination of fluorine in minerals by electron microprobe. Mineralogical Magazine, 53, 357–362.
Raudsepp, M. (1995) Recent advances in the Electron-Probe Micro-Analysis of minerals for the light elements. Canadian Mineralogist, 33, 203–218.
Reed, S.J.B. (1996) Electron Microprobe Analysis and Scanning Electron Microscopy in Geology. Cambridge University Press, Cambridge, U.K.
Robinson, K., Gibbs, G.V., and Ribbe, P.H. (1971) Quadratic elongation: a quantitative measure of distortion in coordination polyhedra. Science, 172, 567–570.
Sheldrick, G.M. (1993) SHELXL-93: Program for Crystal Structure Refinement. University of Göttingen, Germany.
Solberg, T.N. (1982) Fluorine electron microprobe analysis: variations of X-ray peak shape. In K.F.J. Heinrich, Ed., Microbeam Analysis, 148–150. San Francisco Press, Inc., San Francisco, California.
Stormer, F.C. Jr., Pierson, M.L., and Tacker, R.C. (1993) Variation of F and Cl X-ray intensity due to anisotropic diffusion in apatite during electron microprobe analysis. American Mineralogist, 78, 641–648.
Taylor, W.H. and West, J. (1928) The crystal structure of chondrodite series. Proceedings of the Royal Society of London, 117, 517–532.
———(1929) The structure of norbergite. Zeitschrift für Kristallographie, 70, 461–474.
Ungaretti, L., Lombardo, B., Domeneghetti, C., and Rossi, G. (1983) Crystal-chemical evolution of amphiboles from eclogitised rocks of the Sesia-Lanzo Zone, Italian Western Alps. Bulletin de Mineralogie, 106, 645–672.
Williams, P. (1992) Quantitative analysis using sputtering techniques: secondary ion and sputtered neutral mass spectrometry. In D. Briggs, M.P. Seah, Eds., Practical Surface Analysis (2nd ed.), 177–228. John Wiley & Sons, New York, USA.
Wilson, A.I.C., Ed. (1992) International tables for X-ray cyrstallography. Kluwer Academic Publishers, Dordrecht, Boston.
Wunder, B., Rubie, D.C., Ross, C.R., II, Medenback, O., Seifert, F., and Schreyer, W. (1993) Synthesis, stability and properties of $Al_2SiO_4(OH)_2$: A fully hydrated analogue of topaz. American Mineralogist, 78, 285–297
Yamamoto, K. (1977) Hydroxyl-chondrodite. Acta Crystallographica, B33, 1481–1485.

MANUSCRIPT RECEIVED JULY 31, 1998
MANUSCRIPT ACCEPTED AUGUST 8, 1999
PAPER HANDLED BY ROBERT J. TRACY